Math Geosci (2022) 54:225–241
https://doi.org/10.1007/s11004-021-09966-6

Sensitivity Analysis of Discrete Fracture Network Connectivity Characteristics

Dmitriy Kolyukhin[1]

Received: 30 December 2019 / Accepted: 17 July 2021 / Published online: 3 August 2021

Abstract This paper presents the results of a sensitivity analysis of the characteristics of discrete fracture network (DFN) connectivity. The sizes of the maximum and mean clusters comprising the DFN and the distribution of the connectivity index were estimated. Attention was primarily directed to the global sensitivity analysis of these characteristics. Sobol sensitivity indices were used to determine the relative contribution of the DFN model parameter uncertainty to the total uncertainty of the studied problem. Dominant Sobol indices for different DFN models and each fracture connectivity characteristic were determined. The analysis of the results allowed the identification of the parameters whose relevant probability distributions are most important for the correct description of the studied statistical model.

Keywords Discrete fracture network · Sensitivity analysis · Sobol indices · Connectivity index

1 Introduction

The spatial distribution of fracture systems and fracture connectivity is important in many geoscience problems. For example, the distribution can significantly affect DFN hydraulic properties (De Dreuzy et al. 2001, 2004; Lei et al. 2017) and seismic wave propagation through subsurface reservoirs (Novikov and Lisitsa 2018). Rubino et al. (2017) found that the connectivity of fractures can reduce the velocity anisotropy. Hunziker et al. (2018) and Caspari et al. (2019) further studied the dependence of seismic attenuation on fracture connectivity.

✉ Dmitriy Kolyukhin
KolyukhinDR@ipgg.sbras.ru

[1] Sobolev Institute of Mathematics SB RAS, Koptug ave. 4, Novosibirsk, Russia 630090

Due to the complex nature of fractured reservoirs and the lack of observational data, a fully deterministic description of fracture system geometry is usually impossible. Therefore, a statistical approach is often used to generate a statistical ensemble of realizations of fracture systems (Xu and Dowd 2010; Miyoshi et al. 2018). This approach allows not only estimation of the average values of the interest quantities but also evaluation of the corresponding probability distributions. For example, it can be used in uncertainty quantification (Berrone et al. 2018) or sensitivity analysis (Jafari and Babadagli 2009; Kolyukhin 2018).

Many studies are devoted to the characterization of statistical DFN models, including analysis of fracture sizes, orientations, spacing, and spatial positions (Baecher et al. 1977; Long et al. 1982; Massart et al. 2010; Miyoshi et al. 2018). For example, De Dreuzy et al. (2001) investigated the influence of power-law distribution parameters of fracture lengths on DFN connectivity. The dependence of DFN permeability on the spatial correlation of fracture centers was studied by De Dreuzy et al. (2004). In a study by Cacas et al. (1990), the stochastic model of a fracture network in crystalline rocks was developed to investigate potential nuclear waste repository sites. Several statistical models of rock-joint systems were suggested in a study by Dershowitz and Einstein (1988). Most of the general approaches to statistical simulation of statistical DFN models are described by Dowd et al. (2007) and Xu and Dowd (2010). Examples of explicit statistical DFN modeling are described by Min et al. (2018) and Protasov et al. (2019).

Many works are devoted to natural fracture systems using fractals and multifractals, which describe the spatial distribution of fractures (e.g., Bonnet et al. 2001; Bour et al. 2002). In particular, this approach allows statistically describing such a phenomenon as the clusterization of fractures (Schueller et al. 2013). Ouillon and Sornette (1996), Bour et al. (2002) and Du Bernard et al. (2002) studied fracture systems in Saudi Arabia, Norway, and Egypt. Analysis of these fracture systems at different scales and estimation of fractal dimensions confirmed the fractal nature of these geological objects. Later, such studies were conducted by Rouai (2016) and Cai et al. (2017). This study followed Darcel et al. (2003) by applying a similar approach to consider the positions of the fracture centers as a fractal set.

Sensitivity analysis (SA) was intended to demonstrate how different parameters affect the modeling results. Traditional approaches are local methods based on the calculation of the perturbations around some state of parameters. The purpose of global sensitivity analysis (GSA) is to study the relative impact of different sources of uncertainty in the model input parameters on the uncertainty of the model output (Saltelli 2005). GSA is typically used to study complex nonlinear models and may determine significant and insignificant parameters, reduce the problem's dimensionality and improve the understanding of the model's behavior (Reuter and Liebscher 2008). This work applies the GSA approach based on Sobol indices (Sobol 2001). These indices allow us to estimate the relative contribution of the model parameter uncertainty to the total variance of the solution. The advantage of this method is the ability to consider the influence of individual parameters and their interaction. The effective Monte Carlo method for numerical estimation of the Sobol indices was developed by Sobol et al. (2007).

In this study, GSA was applied to study the uncertainty of DFN connectivity characteristics such as cluster size and connectivity index. The distribution of the clusters composing the DFN is its significant characteristic. The size of fracture clusters in seismic waves was studied by Hunziker et al. (2018). For example, Hirthe and Graf (2015) used the sizes of fracture clusters as parameters in the statistical modeling of DFNs. The connectivity index (CI) is another essential statistical property of the DFN that quantifies the connectivity between any two spatial points in the reservoir (Xu et al. 2006). Novikov and Lisitsa (2018) studied the dependence of seismic attenuation on the CI. Wang et al. (2018) showed the significant impact of the CI on shale gas production.

This paper aimed to develop a methodology for determining the parameters of a DFN statistical model whose probability distributions are essential for reproducing the considered attributes of fracture connectivity.

2 Statistical Modeling of DFN

This study investigated the statistical models of DFN. The models are described by parameters that specify the probability distributions of a center's positions, lengths, and orientation of the fractures. This approach allows explicit statistical modeling of the geometry of DFNs (Xu and Dowd 2010). In particular, fracture centers are generated from a fractal spatial density distribution defined by its fractal dimension. In contrast, fracture orientations and lengths are described by normal, lognormal, or power-law distributions. The general methods for statistical modeling of random variables with given probability distributions are described by Rubinstein (1981).

Multifractals are generalizations of fractals. In general, their spatial distribution is characterized by an infinite multifractal spectrum (Xie et al. 1999)

$$D_{-\infty} \geq \cdots \geq D_0 \geq \cdots \geq D_{\infty}. \tag{1}$$

In this study, the distribution of the fracture centers was modeled as a monofractal set for which the dimensions shown in Eq. (1) should be equal.

In the fractal and multifractal models, the studied domain was covered by a regular grid of linear mesh size ϵ. The i-th cell is characterized by the probability $p_i(\epsilon)$ that an arbitrary fracture center $\mathbf{x_j}$, $1 \leq j \leq N$ falls in this cell. Multifractal dimensions are defined as (Xie et al. 1999)

$$D_q = \begin{cases} \frac{1}{q-1} \lim_{\epsilon \to 0} \frac{\ln\left(\sum_{i=1}^{N(\epsilon)} p_i^q(\epsilon)\right)}{\ln \epsilon}, & q \neq 1 \\ \lim_{\epsilon \to 0} \frac{\sum_{i=1}^{N(\epsilon)} p_i(\epsilon) \ln p_i(\epsilon)}{\ln \epsilon}, & q = 1 \end{cases}. \tag{2}$$

Particular attention in this study was paid to dimension D_2, which is also called the correlation dimension. Grassberger and Procaccia (1983) suggested the efficient method of D_2 estimation based on using Eqs. (3) and (4)

$$C_2(r) = \lim_{N \to \infty} \frac{2}{N(N-1)} \sum_{i<j} \Theta(r - |\mathbf{x_i} - \mathbf{x_j}|), \tag{3}$$

$$D_2 \approx \frac{\ln C_2(r)}{\ln r}. \tag{4}$$

Here, N is the total number of fractures, $\mathbf{x}$ is a fracture's position, r is a distance, $C_2(r)$ is a pair correlation function, and $\Theta(r)$ is the Heaviside function whose value is zero if the argument is negative or otherwise one. In the one-dimensional case, the D_2 values estimated by Du Bernard et al. (2002) were 0.87±0.05 and 0.84±0.06 by Schueller et al. (2013). Bour et al. (2002) estimated the two-dimensional correlation dimension D_2 to be 1.77.

In this study, Eq. (5) was restricted with order $q = 2$. The iterative cascade algorithm described by Darcel et al. (2003) was employed for the simulation of the fracture centers' spatial distribution. The whole studied domain is divided into equal cells, and the probability value corresponding to the frequency of fracture centers is assigned to each cell. The simulation began with one cell coinciding with the entire domain, which was assigned probability value of $P = 1$. At the start of any iteration, each subdomain dimension was divided into four equal parts. If the probability assigned to the original subdomain equaled P, then the probabilities of the resulting subdomains were $PP_1, \ldots, PP_4$, in random order. The probabilities $P_1, \ldots, P_4$ were defined by conditions $P_1 + \cdots + P_4 = 1$, $P_1, \ldots, P_4 \geq 0$ and the following equation

$$\sum_{i=1}^{4} \frac{P_i^2}{\left(\frac{1}{2}\right)^{D_2}} = 1. \tag{5}$$

The fragmentation procedure for the first and second iterations is illustrated in Fig. 1. Top plots show the first iteration. Bottom plots illustrate the first step of the second iteration consisting of fragmentation of the filled subdomain in the upper right plot. Kolyukhin (2015) employed this algorithm for one-dimensional modeling of the deformation bands' spatial distribution with the fractal distribution extended for $q > 2$.

This study considered two qualitatively different DFN models. Inspired by Long et al. (1982), the first model consists of two families of fractures whose orientation has a normal probability distribution. In this case, the fracture lengths are distributed according to the lognormal distribution.

Based on the analysis of fracture systems conducted by Bahat (1987) and Bonnet et al. (2001), the second DFN model consisted of three sets of fractures with lengths described by a truncated power-law distribution

$$p(L) \sim L^{-\alpha}, \quad L \in [L_{\min}, L_{\max}].$$

The default DFN parameters are shown in Tables 1 and 2. In all models considered in this study, fracture centers were generated in the domain $\Omega = [0, 5m] \times [0, 5m]$. Figure 2 shows the realizations of DFN with the parameters from Tables 1 (left) and 2 (right).

Table 1 Parameters of the first DFN model

DFN parameter values	Set 1	Set 2
Fractures intensity (Number/m^2)	4	4
Fractures orientation $\phi°$. Normal distribution $N(m_\phi, \sigma_\phi)$.	30, 5	150, 5
Fractures length L(m). Lognormal distribution (m_L, σ_L^2)	0.4, 0.1	0.3, 0.075
Correlation dimension D_2	1.75	1.75

Table 2 Parameters of the second DFN model

DFN parameter values	Set 1	Set 2	Set 3
Fractures intensity (Number/m^2)	3	3	3
Fractures orientation $\phi°$. Normal distribution $N(m_\phi, \sigma_\phi)$.	30, 5	60, 5	345, 5
Fractures length. Power-law distribution α	2.1	2.1	2.1
Correlation dimension D_2	1.75	1.75	1.75
$L_{\min}$(m), $L_{\max}$(m)	0.1, 10	0.1, 10	0.1, 10

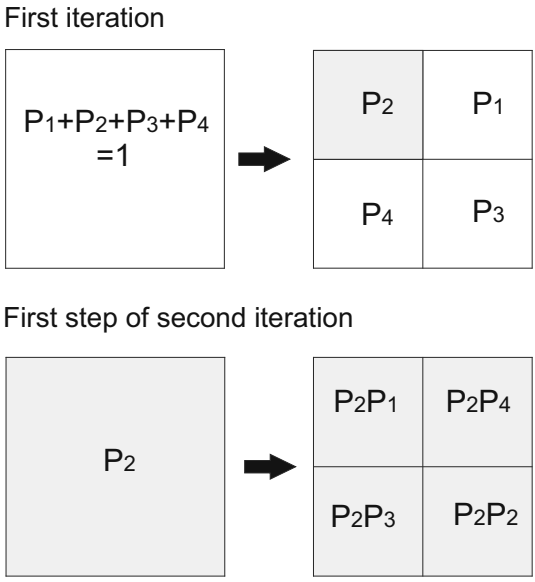

Fig. 1 Simulation of the fracture centers' spatial distribution. Illustration of the modeling scheme suggested in (Darcel et al. 2003, Fig. 1). The first iteration (top plots) and the first step of the second iteration (bottom plots)

3 Global Sensitivity Analysis and Sobol Indices

The purpose of the sensitivity analysis was to estimate the impact of uncertainty caused by random parameter variability on the total uncertainty of the model. In this study, the approach suggested by Sobol (2001) was applied. The proposed method based on

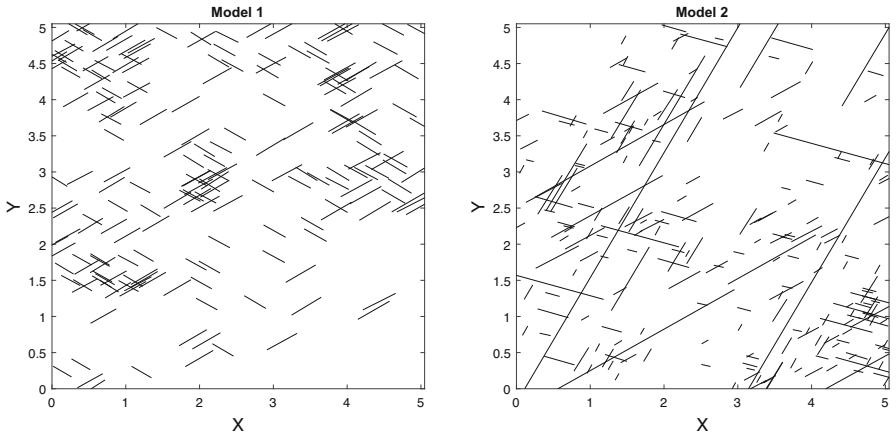

Fig. 2 Examples of DFN realizations with the parameters in Tables 1 (left) and 2 (right)

analysis of variance (ANOVA) uses the decomposition of the integrable function $f(\mathbf{x})$

$$f(x_1,\ldots,x_n) = f_0 + \sum_{i=1}^{n} f_i(x_i) + \sum_{i=1}^{n}\sum_{j=i+1}^{n} f_{i,j}(x_i,x_j) + \cdots + f_{1,\ldots,n}(x_1,\ldots,x_n), \tag{6}$$

where

$$\int f_{i_1,\ldots,i_m}(x_{i_1},\ldots,x_{i_m})dx_k = 0, \quad k = i_1,\ldots,i_m, \tag{7}$$

and the Sobol sensitivity indices are defined as

$$S_{i_1,\ldots,i_m} = \frac{V_{i_1,\ldots,i_m}}{V}. \tag{8}$$

Here, V is the total variance

$$V = \int f^2(\mathbf{x})\mathrm{d}\mathbf{x} - f_0^2, \tag{9}$$

and variances $V_{i_1,\ldots,i_m}$ have the form

$$V_{i_1,\ldots,i_m} = \int f^2_{i_1,\ldots,i_m}(x_{i_1},\ldots,x_{i_m})\mathrm{d}x_1\ldots\mathrm{d}x_m. \tag{10}$$

This approach allowed the ranking of the model parameters by the relative impact on the variance of the solution to the problem.

The Sobol indices defined by Eq. (8) were estimated using the Monte Carlo method developed by Sobol et al. (2007). Table 3 shows the parameters of the DFN model considered in the sensitivity analysis. The numbering of the parameters in this table denotes the Sobol indices $S_{i_1,\ldots,i_m}$.

All model parameters were divided into two subsets

$$\mathbf{x} = (\mathbf{y},\mathbf{z}). \tag{11}$$

Table 3 Parameters of the DFN model used for the sensitivity analysis

DFN parameters	Parameter number
The positions of the fracture centers	1
Fractures length L	2
Fractures orientation ϕ	3

In the first step of the employed method, it is necessary to generate the N_R realizations of the set of $2n$ independent random values

$$(\xi, \eta), (\xi', \eta'), k = 1, \ldots, N. \tag{12}$$

The estimation of variance V_y has the form

$$V_y \approx \frac{1}{N} \sum_{k=1}^{N} f(\xi, \eta) \left(f(\xi, \eta') - f(\xi', \eta') \right). \tag{13}$$

The standard estimation of Monte Carlo error is applied to evaluate the accuracy of numerical computations. 95% confident interval for statistical estimation ξ has the form

$$S_{i_1,\ldots,i_m} \pm 1.96 \frac{\sigma_\xi}{\sqrt{N_R}}, \tag{14}$$

where σ_ξ is a standard deviation of ξ.

4 Cluster Size Sensitivity Analysis

This section describes the analysis of the fracture cluster sizes. Statistical modeling was employed to generate an ensemble of N_R DFN realizations. Each generated DFN was divided into nonintersecting clusters of intersecting fractures. The maximum and mean cluster sizes were estimated for each realization. Cluster size (CL) was the longest in the X or Y direction. Furthermore, these values were averaged over the ensemble as the arithmetic means of the values for each realization. The primary goal was to analyze the sensitivity of these cluster sizes to the model parameters. The dependencies of the significant Sobol indices on the number of fractures N, the correlation dimension D_2, the parameters of fracture length distribution, and the standard deviation of fracture orientation distribution σ_ϕ were studied. In all computations, the number of realizations was $N_R = 6 \cdot 10^5$.

4.1 Dependence on the Number of Fractures

Figure 3 shows the dependencies of the mean value $< \mathrm{CL} >$ and standard deviation $\sigma(\mathrm{CL})$ of the maximum and average cluster sizes on the number of fractures N. The figure shows that the maximal cluster size increases with an increase in the number of

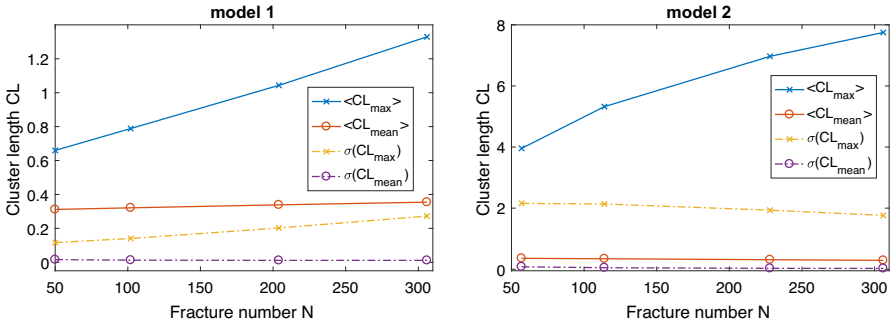

Fig. 3 The dependence of the mean value and standard deviation of the maximum (CL_{max}) and average (CL_{mean}) cluster sizes on the number of fractures for Model 1 (left) and Model 2 (right)

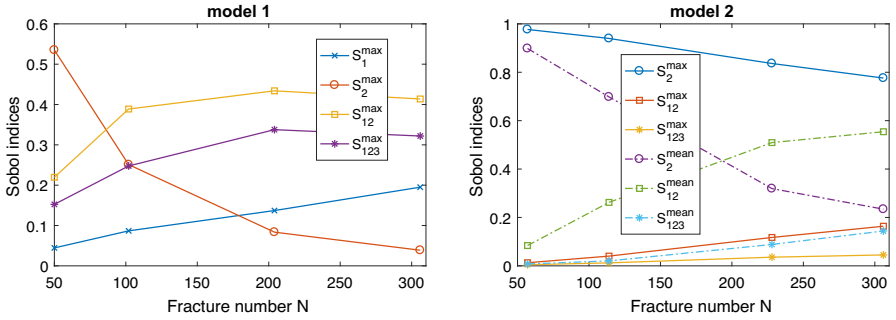

Fig. 4 The dependence of significant sensitivity indices for the maximum (S^{max}) and average (S^{mean}) cluster sizes on the number of fractures for Model 1 (left) and Model 2 (right)

fractures for both models. On the other hand, other characteristics in these plots are less dependent on N. For example, the average cluster size for the second model does not increase with an increase in the number of fractures. This is due to an increase in the number of small clusters and unconnected fractures. As shown in the left plot in Fig. 3, the standard deviation does not exceed 5% of the mean for the average cluster size (circle markers). Therefore, here and below in Sect. 4, for the first model, the sensitivity analysis was performed only for the size of the maximum cluster.

The dependence of the significant sensitivity indices on the number of fractures is shown in Fig. 4. For this and other dependencies in Sect. 4, S_1, S_2, S_{12}, and S_{123} are the significant indices for the first model, whereas S_2, S_{12}, and S_{123} are the significant indices for the second model. For all of the models, the S_2 index decreases with increasing N. This means that with an increase in the number of fractures, the number of intersections increases, and the structure of the DFN becomes more complex. This increases the importance of the mixed S_{12} and S_{123} indices. On the other hand, the first-order index S_2 is still dominant in the second model because of the long fractures generated according to the power-law distribution. The exception is the average cluster size for the second model and large N values. In this case, the mixed S_{12} index is dominant.

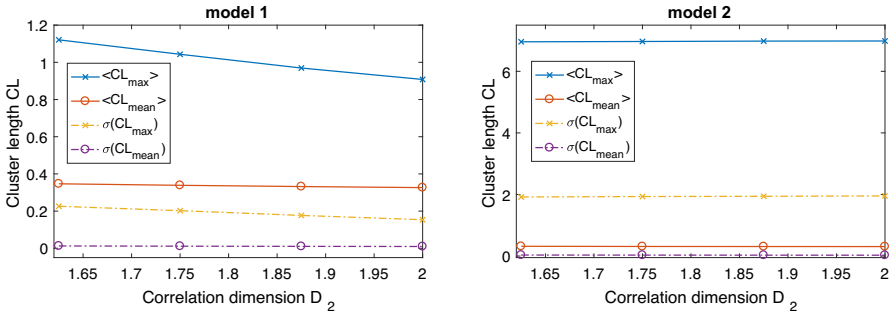

Fig. 5 The dependence of the mean and standard deviation on the maximum (CL_{max}) and the average (CL_{mean}) cluster sizes on the correlation dimension D_2 for Model 1 (left) and Model 2 (right)

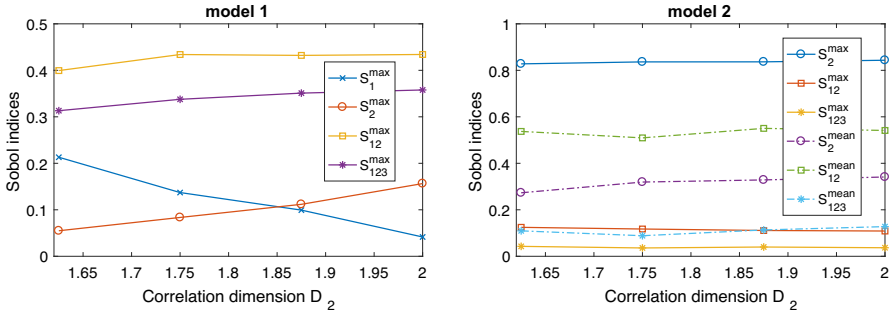

Fig. 6 The dependence of significant sensitivity indices for the maximum (S^{max}) and average (S^{mean}) cluster sizes on the correlation dimension D_2 for Model 1 (left) and Model 2 (right)

4.2 Dependence on the Correlation Dimension D_2

The left plot in Fig. 5 shows that the mean values of the maximum and average cluster sizes decrease with increasing D_2, corresponding to a more uniform distribution of fracture centers. The left plot in Fig. 6 shows that the S_1 index decreases and the S_2 index increases as D_2 increases. The effect is that the distribution of fracture centers makes a more significant contribution to the total dispersion under increased clustering. In contrast, the length distribution results in a greater impact on the uniform distribution of the fracture centers. At the same time, the dominant mixed indices S_{12} and S_{123} are less dependent on the correlation dimension.

On the other hand, on the right plots in Figs. 5 and 6, the studied characteristics do not depend on D_2. This may result from the greater complexity of the second model due to the more significant number of fracture sets and the greater scatter of fracture lengths. The degree of clustering of the centers of the fractures no longer affects the results of the sensitivity analysis.

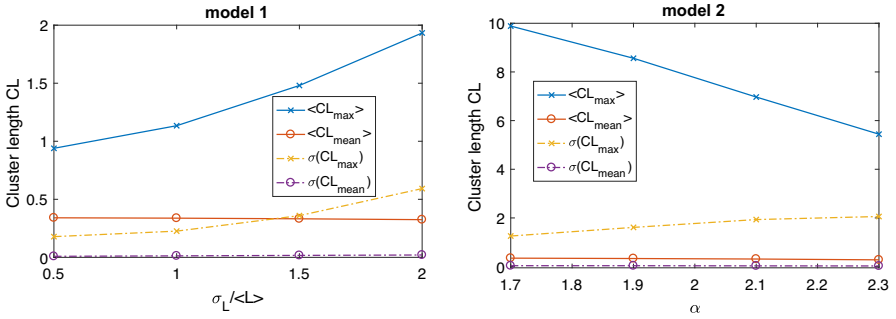

Fig. 7 The dependence of the mean and standard deviation of the maximum (CL_{max}) and average (CL_{mean}) cluster sizes on the parameters σ_L for Model 1 (left) and α for Model 2 (right)

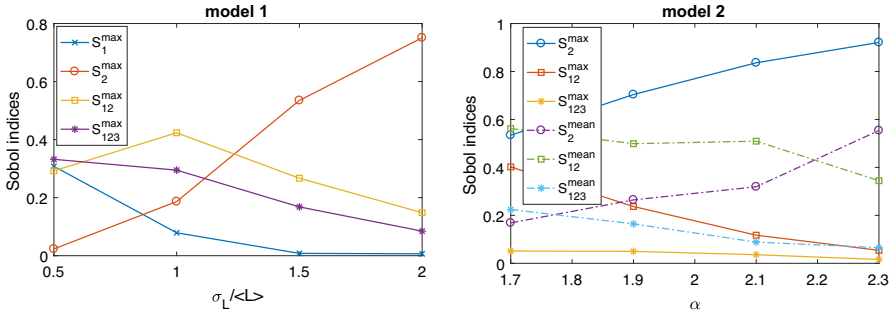

Fig. 8 The dependence of significant sensitivity indices for the maximum (S^{max}) and average (S^{mean}) cluster sizes on the parameters σ_L for Model 1 (left) and α for Model 2 (right)

4.3 Dependence on Fracture Length Distribution

An increase in the standard deviation σ_L in Fig. 7 (left plot) leads to an increase in the maximum cluster size. For the second model (right plot), the maximum cluster size increases with decreasing α value, corresponding to an increase in the number of long fractures. In turn, the average cluster size does not depend on the parameters of the fracture length distribution, similar to the dependencies in Fig. 3.

As shown in Fig. 8, S_2 values increase with the increase in σ_L and α. In the left plot, this coincides with an increase in the variance of the fracture length. On the other hand, in the right plot, S_2 increases with a decrease in the values of the mathematical expectation and the variance of the fracture length. This shows a more complex dependence of CL uncertainty on the fracture length for the second model. Perhaps this is because, with a decrease in the length of individual fractures, the number of intersections decreases. In turn, this leads to a reduction in the contribution of the mixed indices.

4.4 Dependence on the Variance in the Distribution of Fracture Orientation

Sensitivity indices were also estimated for different values of σ_ϕ. Figure 9 shows that <CL> and σ(CL) do not depend on the variance of fracture orientation. However, as shown in Fig. 10 the value of index S_{123} increases with an increase in the standard deviation σ_ϕ. Thus, the contribution of orientation to the model uncertainty appears in the behavior of the index describing the mixed impact of all three parameters.

Figure 3 through 10 show only the significant sensitivity indices whose values significantly exceeded the statistical error of the numerical computations. For comparison, Fig. 11 shows the Sobol indices $S_{13}^{\max}$ and S_1^{mean} compared with the statistical error estimated by Eq. (14) for the first and second models. The right plot shows that S_1^{mean} may exceed 5%, but those values are comparable with the related statistical error.

5 Sensitivity Analysis of the Connectivity Index

The CI (connectivity index) $\tau(\mathbf{x}, \mathbf{y})$, a characteristic of DFN connectivity, was introduced by Xu et al. (2006). $\tau(\mathbf{x}, \mathbf{y})$ is equal to the probability that fractures connect

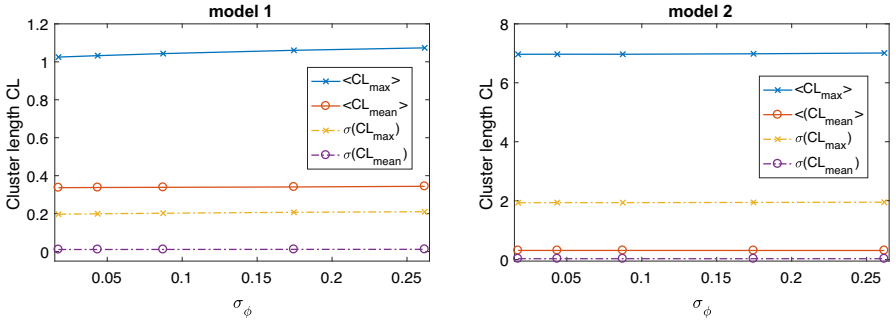

Fig. 9 The dependence of the mean and standard deviation of the maximum (CL_{max}) and average (CL_{mean}) cluster sizes on σ_ϕ for Model 1 (left) and Model 2 (right)

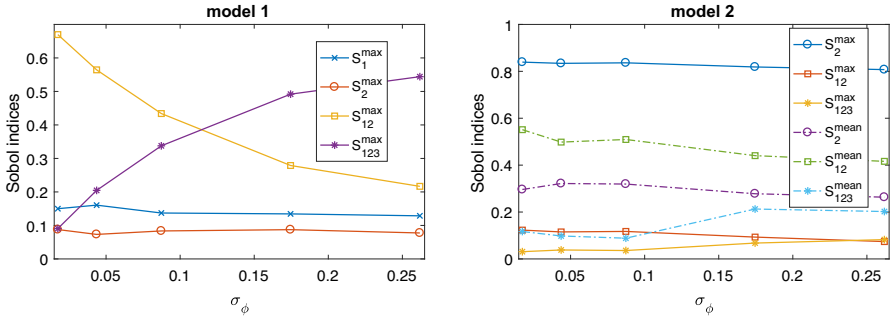

Fig. 10 The dependence of significant sensitivity indices for the maximum ($S^{\max}$) and average (S^{mean}) cluster sizes on σ_ϕ for Model 1 (left) and Model 2 (right)

points **x** and **y**

$$\tau(\mathbf{x}, \mathbf{y}) = \mathbf{P}(\mathbf{x} \leftrightarrow \mathbf{y}). \tag{15}$$

The CI values between the central cell and the surrounding cells were estimated in this study. The estimated values were averaged over the number of statistical DFN realizations. Figure 12 illustrates the CI and the total variance V of the two models.

The major Sobol indices for the CI are shown in Fig. 13 for the first model and 14 for the second model. These figures show that the indices are distributed differently in the modeling domain. S_1 and S_{12} are the significant sensitivity indices for the CI of the first models. Figure 13 shows the values of these sensitivity indices in the domain where the variance is not less than 1% of its maximum value. From this plot, it is clear that the τ uncertainty for this model is almost fully determined by the uncertainty in the fracture center positions.

The significant sensitivity indices of τ for the second DFN model are S_1, S_{12}, S_{13}, and S_{123}. Figure 14 shows these indices in the domain where the variance is not less than 5% of its maximum value. The figure shows that index S_1 is dominant in the central part of the studied domain only. This means that this model parameter primarily affects the variance of the CI of cells that are close to each other. As the distance between cells increases, this dependence becomes more complex, and the uncertainty of the CI is determined by the Sobol indices S_{12} and S_{123}. The parameters describing fracture lengths and orientations are also significant.

6 Conclusions

In this study, a numerical sensitivity analysis of two qualitatively different statistical DFN models (Figs. 2 and 3) was conducted with the parameters shown in Tables 1 and 2. The values of the maximum and mean cluster sizes constituting the DFN were investigated. The global Sobol sensitivity indices characterizing the contribution of the uncertainty of the model parameters to the total uncertainty of the considered functions were estimated. The dependencies of the sensitivity indices on the main parameters of the statistical models were studied.

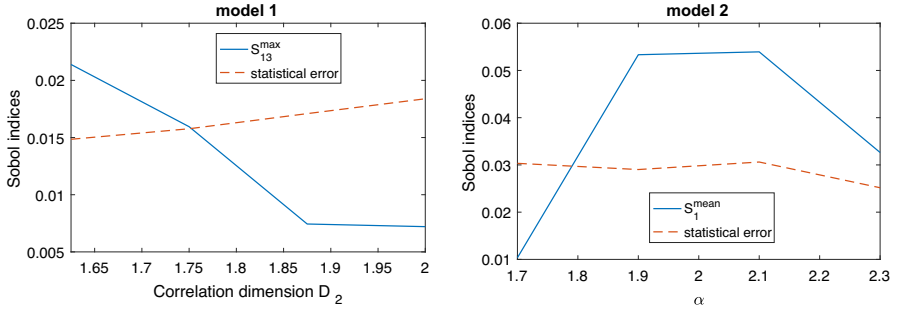

Fig. 11 The dependence of the sensitivity indices $S_{13}^{\max}$ and S_1^{mean} and the corresponding statistical errors on D_2 (model 1) and α (model 2)

In the case of cluster sizes, the sensitivity indices behave differently in the two models. S_2, S_{12}, and S_{123} are the significant indices for both models. In the first model, considering the maximum cluster size, index S_1 also becomes meaningful. In the second model, the Sobol index S_2 is dominant because of the longer length of fractures. On the other hand, in the first model, indices S_{12} and S_{123} show the highest values. However, with a decrease in the number of fractures and an increase in σ_L, indices S_1 and S_2 become dominant.

The analysis showed that the Sobol indices are weakly dependent on the correlation dimension D_2 (Fig. 6), which describes the clustering of the fracture centers. An exception is indices S_1 and S_2 for the maximum cluster size in the first DFN model. Mixed indices S_{12} and S_{123} are the most sensitive to variation in fracture orientation variance (Fig. 10, left graph). S_{12} decreases and S_{123} increases with increasing σ_ϕ. As shown in the right plot of Fig. 10, the curves corresponding to S_{123} also increase, although it is less pronounced. In contrast, S_3 remains negligible. This indicates an implicit increase in the orientation influence described by the mixed index S_{123}.

Numerical experiments showed a more complex dependence of the sensitivity indices on the number of fractures and fracture length variance σ_L^2. As a result, we conclude that for the models, the primary contributor to the uncertainty of the prob-

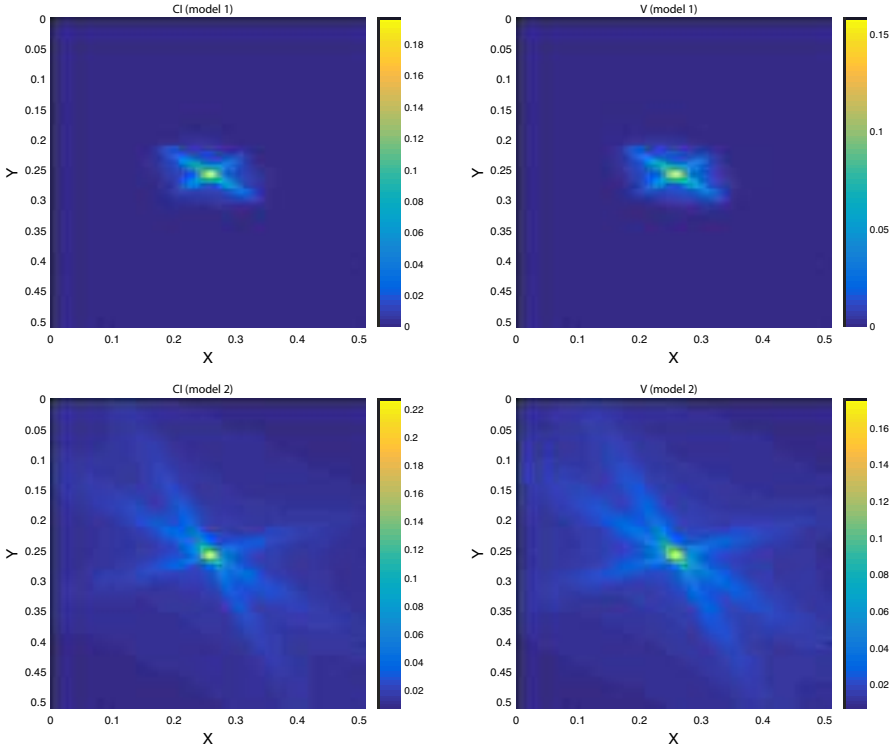

Fig. 12 The spatial distribution of the CI (left) and its total variance V (right) for Model 1 (top) and Model 2 (bottom)

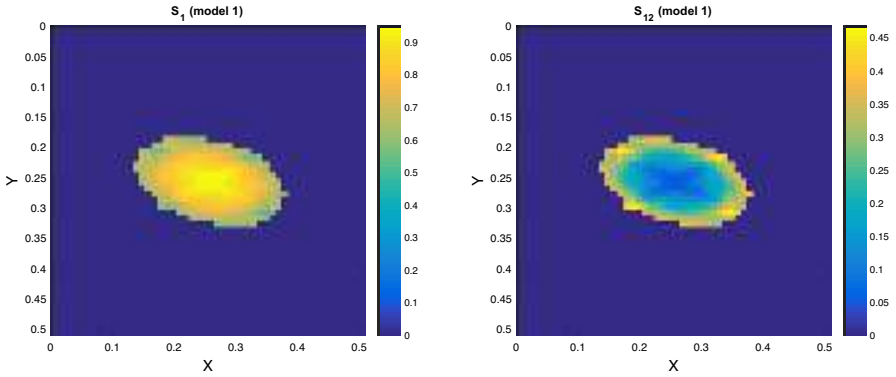

Fig. 13 The spatial distribution of the significant sensitivity indices S_1 and S_{12} for the CI in Model 1

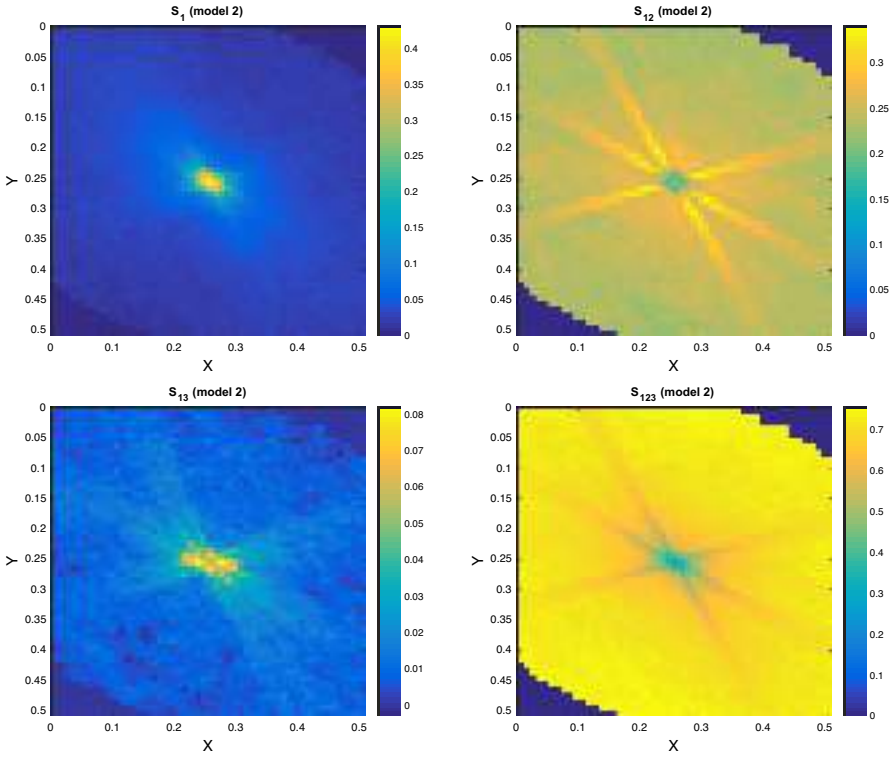

Fig. 14 The spatial distribution of the significant sensitivity indices S_1, S_{12}, S_{13} and S_{123} for the CI in Model 2

lem is the uncertainty of fracture lengths. The influence of the uncertainty of the other parameters is indirect and described by the mixed Sobol indices S_{12} and S_{123}. However, as described in Sect. 4, index S_1 describing the impact of the fracture position uncertainty is also significant in some cases.

In the second part of this study, the connectivity index was evaluated, and the corresponding sensitivity analysis was performed (Figs. 12, 13, 14). As with cluster sizes, the sensitivity indices behave differently in the two DFN models. Moreover, different indices determined the uncertainty of the CI in other subdomains. For both models, the sensitivity index S_1 determined by the position of the fracture centers is the predominant value for the connectivity index of the close points. As the distance between the points increases, the distributions of lengths (for both models) and the orientation of fractures (for the second model) also become more significant.

In general, we can conclude that the complication of the model (for example, an increase in the number of families or intersection of fractures) increases the number of significant Sobol indices and the relative contribution of mixed indices characterizing the interaction of model parameters. The results presented in this study can be helpful for efficient statistical DFN modeling. They promote a qualitative understanding of the parameters essential for the accurate description of the problem uncertainty.

Acknowledgements Financial support from the Russian Science Foundation (Grant No. 19-77-20004) is gratefully acknowledged. The author would like to thank the editor and two anonymous reviewers for their constructive comments on the earlier version of the manuscript.

References

Baecher G, Lanney NA, Einstein HH (1977) Statistical description of rock properties and sampling. In: 18th U.S. symposium on rock mechanics (USRMS), Golden, Colorado

Bahat D (1987) Jointing and fracture interactions in Middle Eocene chalks near Beer Sheva, Israel. Tectonophysics 136:299–321

Bonnet E, Bour O, Odling NE, Davy P, Main I, Cowie P, Berkowitz B (2001) Scaling of fracture systems in geological media. Rev Geophys 39(3):347–383

Bour O, Davy P, Darcel C (2002) A statistical scaling model for fracture network geometry, with validation on multiscale mapping of a joint network (Hornelen Basin, Norway). J Geophys Res 107:B6

Berrone S, Canuto C, Pieraccini S, Scialo S (2018) Uncertainty quantification in discrete fracture network models: stochastic geometry. Water Resour Res 54(2):1338–1352

Cacas MS, Ledoux E, de Marsily G, Tillie B, Barbreau A, Durand E, Feuga B, Peaudecerf P (1990) Modeling fracture flow with a stochastic discrete fracture network: calibration and validation: 1. The flow model. Water Resour Res 26(3):479–489

Cai J, Wei W, Hu X, Liu R, Wang J (2017) Fractal characterization of dynamic network extension in porous media. Fractals 25(2):1750023

Caspari E, Novikov M, Lisitsa V, Barbosa ND, Quintal B, Rubino JG, Holliger K (2019) Attenuation mechanisms in fractured fluid-saturated porous rocks: a numerical modelling study. Geophys Prosp 67(4):935–955

Darcel C, Bour O, Davy P, de Dreuzy JR (2003) Connectivity properties of two-dimensional fracture network with stochastic fractal correlation. Water Resour Res 39(10):1272

Davy P, Sornette A, Sornette D (1990) Some consequences of a proposed fractal nature of continental faulting. Nature 348:56–58

De Dreuzy JR, Davy P, Bour O (2001) Hydraulic properties of two-dimensional random fracture networks following a power law length distribution 1. Effective connectivity. Water Resour Res 37(8):2065–2078

De Dreuzy JR, Darcel C, Davy P, Bour O (2004) Influence of spatial correlation of fracture centers on the permeability of two-dimensional fracture networks following a power law length distribution. Water Resour Res 40:W01502

Dershowitz WS, Einstein HH (1988) Characterizing rock joint geometry with joint system models. Rock Mech Rock Eng 21:21–51

Dowd PA, Xu C, Mardia KV, Fowell RJ (2007) A comparison of methods for the stochastic simulation of rock fractures. Math Geol 39:697–714

Du Bernard X, Labaume P, Darcel C, Davy P, Bour O (2002) Cataclastic slip band distribution in normal fault damage zones, Nubian sandstones. Suez rift. J Geophys Res 107:B7

Grassberger P, Procaccia I (1983) Measuring the strangeness of strange attractors. Physica D: Nonlinear Phenomena 9(1–2):189–208

Hirthe EM, Graf T (2015) Fracture network optimization for simulating 2D variable-density flow and transport. Adv Water Resour 83:364–375

Hunziker J, Favino M, Caspari E, Quintal B, Rubino JG, Krause R, Holliger K (2018) Seismic attenuation and stiffness modulus dispersion in porous rocks containing stochastic fracture networks. J Geophys Res 123(1):125–143

Jafari A, Babadagli T (2009) A sensitivity analysis for effective parameters on 2D fracture-network permeability. SPE Reserv Eval Eng 12(3):455–469

Kolyukhin DR (2015) Statistical simulation technique for deformation band spatial distribution in the fault damage zone. Sib Electron Math Rep 12:465–479

Kolyukhin D (2018) Global sensitivity analysis for a stochastic flow problem. Monte Carlo Methods Appl 24(4):263–270

Lei Q, Latham JP, Tsang CF (2017) The use of discrete fracture networks for modelling coupled geomechanical and hydrological behaviour of fractured rocks. Comput Geotech 85:151–176

Long JCS, Remer JS, Wilson CR, Witherspoon PA (1982) Porous Media Equivalents for Networks of Discontinuous Fractures. Water Resour Res 18(3):645–658

Massart B, Paillet M, Henrion V, Sausse J, Dezayes C, Genter A, Bisset A (2010) Fracture Characterization and Stochastic Modeling of the Granitic Basement in the HDR Soultz Project (France). World Geothermal Congress 2010 Bali, Indonesia, 25-29 April 2010

Min KB, Jing L, Stephansson O (2018) Determining the equivalent permeability tensor for fractured rock masses using a stochastic REV approach: Method and application to the field data from Sellafield. UK. Hydrogeology J 12(5):497–510

Miyoshi T, Elmo D, Rogers S (2018) Influence of data analysis when exploiting DFN model representation in the application of rock mass classification systems. J Rock Mech Geotechnical Eng 10(6):1046–1062

Novikov M, Lisitsa V (2018) From percolation of fractured media to seismic attenuation: a numerical study. In: 6th international conference integrity-reliability-failure Lisbon/Portugal 22–26 July 2018

Ouillon G, Sornette D (1996) Unbiased multifractal analysis: application to fault patterns. Geophys Res Lett 23(23):3409–3412

Protasov MI, Khachkova TS, Kolyukhin DR, Bazaikin YV (2019) Characterization of fractured zones via topological analysis of 3D seismic diffraction images. Geophysics 84(5):1SO-Z28

Reuter U, Liebscher M (2008) Global sensitivity analysis in view of nonlinear structural behavior. LSDYNA Anwenderforum, Bamberg

Rouai M (2016) Multifractal Properties of Fracture Network in Sefrou Carbonate Reservoir (Morocco). In: 78th EAGE conference and exhibition, pp 1-5

Rubino JG, Caspari E, Muller TM, Holliger K (2017) Fracture connectivity can reduce the velocity anisotropy of seismic waves. Geophys J Int 210(1):223–227

Rubinstein RY (1981) Simulation and the Monte Carlo method. Wiley, New York

Saltelli (2005) Global sensitivity analysis: an introduction. In: Hanson KM, Hemez FM (eds) sensitivity analysis of model output. Los Alamos National Laboratory

Sobol' IM (2001) Global sensitivity indices for nonlinear mathematical models and their Monte Carlo estimates. Math and Comput Simul 55(1–3):271–280

Sobol' IM, Tarantola S, Gatelli D, Kucherenko SS, Mauntz W (2007) Estimating the approximation error when fixing unessential factors in global sensitivity analysis. Reliab Eng Syst Saf 92(7):957–960

Schueller S, Braathen A, Fossen H, Tveranger J (2013) Spatial distribution of deformation bands in damage zones of extensional faults in porous sandstones: statistical analysis of field data. J Struct Geol 52:148–162

Wang L, Dong Z, Li X, Xia Z (2018) A multi-scale flow model for production performance analysis in shale gas reservoirs with fractal geometry. Sci Rep 8:11464
Xie H, Wang JA, Kwasniewski MA (1999) Multifractal characterization of rock fracture surfaces. Int J Rock Mech Min Sci 36:19–27
Xu C, Dowd PA, Mardia KV, Fowell RJ (2006) A connectivity index for discrete fracture network. Math Geol 38(5):611–634
Xu C, Dowd P (2010) A new computer code for discrete fracture network modelling. Math Geosci 36(3):292–301